Available online at www.sciencedirect.com
ScienceDirect
Journal of the European Ceramic Society 31 (2011) 1975–1985
www.elsevier.com/locate/jeurceramsoc

Synthesis and long-term test of borosilicate-based sealing glass for solid oxide fuel cells

Sung-En Lin, Yi-Ru Cheng, W.C.J. Wei *

Dept. Mat. Sci. Eng., National Taiwan University, Taipei 106, Taiwan, ROC

Received 14 November 2010; received in revised form 5 April 2011; accepted 13 April 2011

Abstract

A series of borosilicate-based glasses, ternary $BaO–SiO_2–B_2O_3$ and quaternary $BaO–SiO_2–B_2O_3–Al_2O_3$ systems, are prepared as sealing materials for intermediate temperature solid oxide fuel cells (IT-SOFCs). The thermal expansion, crystalline phases, glass forming ability, and thermo-chemical stabilities of the glasses are characterized. Additionally, the effect of the B_2O_3/SiO_2 ratio and Al_2O_3 and BaO contents on the coefficient of thermal expansion (CTE) are discussed and compared. Test results show that one glass (G6) can fully wet various substrates at the sealing temperature of 1000 °C and match thermal expansion. Possible interfacial reactions between the glass and those cell components aging up to 5000 h are investigated by element mapping, XRD, SEM, and EPMA. Leakage testing was also performed at temperatures up to 650 °C. The results show that the glass (G6) remains amorphous after 5000 h test and is stable under these conditions and compatible with the other fuel cell components.

Keywords: Glass; Silicate; Fuel cells; Borate

1. Introduction

Solid oxide fuel cells (SOFCs) have recently attracted attention as a tool to save energy because of their high energy conversion efficiency and environmental friendliness.[1–3] In order to reduce the fabrication cost of SOFCs, recent research efforts have aimed to decrease the operation temperature from 800 to 1000 °C to an intermediate range, 500–650 °C. To meet this change in operating temperature, the properties of the main components, such as the anode, cathode, and electrolyte, must be improved in this temperature range.[3–12] One of the trials[8] demonstrated that a SOFC cell with very thin YSZ (<1 μm) electrolyte layer can be used as low as 650 °C.

In order to achieve high operation efficiency, the sealing issue in SOFC is important as well. Three key factors for sealing materials should be considered: (i) chemical stability to meet long-term operation requirements; (ii) good mechanical strength to sustain cell structure at the operating temperature; (iii) the high resistivity of the seal to prevent current and gas leakage.[13–18] A suitable sealing material should be chemically inert with respect to other components, and should have a coefficient of thermal expansion (CTE) similar to the parts being sealed. Glasses or glass-ceramics are good candidate materials for this application because they can match the mentioned criteria well by a minor modification of their compositions.

The most common sealants for SOFCs are glass and glass-ceramics. Some materials are demonstrated able to operate for more than 1500 h without significant degradation.[10] Glass synthesis is a mature and complex process that is a competing process between liquid phase and the resulting crystalline phase(s). In this regard, glass-forming ability (GFA) includes liquid-phase stability and reveals the possibility of crystal growth in the testing glass. When glasses have characteristic glass transition temperature (T_g), the temperature of endothermic effect due to first melting (T_l), and initial crystallization temperature (T_x), the relative GFA can be reflected by an universal parameter γ[19]:

$$\gamma \propto \frac{T_x}{T_g + T_l}. \quad (1)$$

The greater the γ value, the better the glass forming ability of the oxide glass system will be. Several other parameters

* Corresponding author. Tel.: +886 2 33661317; fax: +886 2 23634562.
E-mail address: wjwei@ntu.edu.tw (W.C.J. Wei).

0955-2219/$ – see front matter © 2011 Elsevier Ltd. All rights reserved.
doi:10.1016/j.jeurceramsoc.2011.04.017

have also been mentioned in the literature[20–22] for characterizing the glass forming ability. These parameters are often used as a guideline to identify a good formula for making glasses.

CTE is the other key factor for sealing materials, and it is ideally in the range of 10–12 ppm/K to match the CTEs of YSZ and SDC. In borosilicate glasses B_2O_3/SiO_2 ratio plays a crucial role in tailoring their thermal properties, namely, glass transition, glass softening, and CTE.[23–29] Generally, increasing the B_2O_3/SiO_2 ratio results in the reduction of T_g, T_s, and viscosity.[25,28] This phenomenon is due to "boron anomaly effect" which means the conversion of three-coordinated boron to four-coordinated boron. Sohn et al.[24] observed an increase in the CTE value as the B_2O_3/SiO_2 ratio increased from 0.3 to 0.8 in $BaO–Al_2O_3–La_2O_3–B_2O_3–SiO_2$ system.[24] A similar result was reported in $BaO/SrO–Al_2O_3–La_2O_3–B_2O_3–SiO_2$ systems by Fergus[25] when the B_2O_3/SiO_2 ratio was varied from 0 to 8. In other reports of the (BaO, SrO, CaO)/$MgO–B_2O_3–SiO_2$ system, an independent relationship between the CTE and B_2O_3/SiO_2 ratio was found when the B_2O_3/SiO_2 ratio ranged between 0 and 0.25.[25] However, Goel et al.[28] reported results with the opposite trend—their CTE values decreased with an increase in the B_2O_3/SiO_2 ratio over the similar range of 0–0.32. They concluded that the CTE of borate glasses decrease until the addition of 15 wt% B_2O_3. CTE of a glass with a higher B_2O_3 content would increase with the B_2O_3/SiO_2 ratio when the ratio increased from 0.3 to 8.[23–25]

The effects of Al_2O_3 and BaO addition to glass on its CTE value and crystalline behavior have also been investigated. The formation of crystalline Ba- and/or Al-containing phases greatly changes the CTE of glass-ceramic systems due to the formation of AlO_4 tetrahedral bonds or non-bridging oxygen.[29] The formation of crystallites in glass made the CTE value dramatically deviate from the substrate glass of the same composition. The effects of B_2O_3/SiO_2, Al_2O_3 and BaO content on the CTE of various glass systems have been extensive discussed.[30–32]

In this study, sealing materials of $BaO–B_2O_3–SiO_2–Al_2O_3$ quaternary systems are tested in order to examine the properties mentioned earlier. The detailed glass preparation and crystallization kinetic behavior of five compositions (G0–G4) close to $BaSiO_3–BaB_2O_4$ eutectic compound were accomplished and reported in our previous work.[33] Two crystalline phases, $BaSiO_3$ (BS) and $BaAl_2Si_2O_8$ (H), might grow in the glasses and appear very an-isotropic shapes after a few hundred hours annealing at the temperatures between 650 and 800 °C. The glass-ceramics appeared strong residual stresses and poor structural integrity. Therefore, new formulae were developed with an appropriate glass transition temperature (T_g), slightly lower than the highest operation temperature, matched CTE to YSZ electrolyte, good chemical stability and acceptable electric resistivity, and good wettability with the parts being sealed.

A G6 glass with a few percents of Al_2O_3 has the greatest potential keeping amorphous state and the good sealing properties to seal SOFCs. Therefore, the possible interactions between G6 glass with the parts of the fuel cell being sealed in both oxidizing and reducing atmospheres over 5000 h of long-term aging are investigated and discussed.

2. Experimental procedures

Four reagent powders, including $BaCO_3$ (>99.9% purity, J.T. Baker, USA), H_3BO_3 (>99.8%, Riedel de Haën, German), SiO_2 (>99.9%, Harrison-Walker Refractories, Eufaula, AL, USA) and Al_2O_3 (>99.7%, Alcoa Industrial Chemicals, Pittsburgh, PA, USA), were used for the fabrication of G-series glasses. Various contents of reagent-grade $BaCO_3$, H_3BO_3, SiO_2 and Al_2O_3 according to Table 1 were thoroughly dispersed in a turbo-mixer for 20 h in alcohol (10 vol% in solid content). The mixed slurries were then dried using a rotary vacuum evaporator (EYELA, Japan). 20 g of dried powder was then placed in a Al_2O_3 crucible and melted in a furnace at 1300 °C over a period of 30 min. The melt was quenched in de-ionized water at room temperature to produce a glass frit, or cooled on a Cu plate to get bulk samples. All the glass powder used in this study was ground until it could pass through a 200-mesh sieve.

As mentioned, CTE is a key factor that should be concerned for materials to be used in the sealing application. Therefore, the effect of B_2O_3/SiO_2 ratio and crystallization in bulk samples of $BaO–B_2O_3–SiO_2$ glass systems (G0–G4) on the CTE was characterized. Then Al_2O_3 was added into the G1 glass system (as G1A5 and G1A10) to modify the CTE value. To search for better glass systems and to realize the effect of BaO content and B_2O_3/SiO_2 ratio on CTE value in $BaO–B_2O_3–SiO_2$ ternary system, the B_2O_3/SiO_2 ratio was fixed at 0.3, 0.5, 0.79 or 1.0, and also adjusted the amount of BaO. 12 other glass formulae (G5–G16) were prepared. Therefore, we can systematically investigate the CTE distribution in this ternary system. The preliminary results showed that the G6 glass had the best properties and the greatest potential to meet the requirement of SOFCs.

Mass produced G6 glass (M-G6) powder used for further study was prepared by Exojet Co. (Hsin-chu, Taiwan). The powder mixture was melted in a fused Al_2O_3-rich crucible at 1300 °C for 30 min, and the melts were quenched in de-ionized water. The glass frit was then ball-milled by 3Y-ZrO_2 milling media for 20 h, and sieved through a 200-mesh sieve to ensure that the glass particle size was less than 75 μm. Several properties were tested and compared with those of lab-produced G6 glass.

2.1. X-ray diffractometric (XRD) analysis

The as-prepared glasses and the heat-treated samples were characterized using an X-ray Diffractometer (XRD, X'Pert PRO, PANalytical Co., The Netherlands) with Cu Kα radiation to identify the crystalline phases. The applied voltage and current were 45 kV and 40 mA, respectively. The scanning speed was 3°/min at a step of 0.04°.

2.2. Differential thermal analysis (DTA)

DTA (SDT Q600, TA Waters LLC, USA; 1600 DTA, DuPont, USA) was performed at a heating rate of 10 °C/min to investigate the thermal properties, such as the glass transition temperature (T_g), temperature of maximal crystallization rate (T_c) and T_l.[34]

Table 1
Composition (mol%) and CTE of various G-series glasses.

Sample No.	BaO	B_2O_3	SiO_2	Al_2O_3	B_2O_3/SiO_2	CTE	XRD result[a]
G0	50.00	25.00	25.00	0	1.0	12.7	BS, BB_2
G1	50.00	22.00	28.00	0	0.79	11.6	BS, H
G2	50.00	17.00	33.00	0	0.52	7.6[b]	BS, H
G3	50.00	12.00	36.00	0	0.33	7.2[b]	BS, H
G4	50.00	10.00	40.00	0	0.25	11.7	BS, H
G5	32.06	15.68	52.26	0	0.3	10.2	BS_2, H, G
G6	32.40	22.54	45.06	0	0.5	9.8	G
G7	36.53	21.14	42.33	0	0.5	10.7	G
G8	46.56	17.82	35.63	0	0.5	12.2	BS, H, G
G9	32.76	29.68	37.56	0	0.79	5.6	H, G
G10	36.93	27.83	35.24	0	0.79	9.5	BS_2, H, G
G11	41.01	26.04	32.95	0	0.79	11.8	G
G12	46.96	23.41	29.63	0	0.79	12.3	BS, H, G
G13	54.24	20.12	25.56	0	0.79	7.9[b]	G
G14	31.02	34.50	34.48	0	1.0	7.1	BS, G
G15	41.22	29.39	29.39	0	1.0	11.0	BS, H, G
G16	47.18	26.41	26.41	0	1.0	12.5	BS, H, G
G1A5	47.50	20.90	26.60	5.00	0.79	11.5	BS, H
G1A10	45.00	19.80	25.20	10.00	0.79	10.2	BS, H

[a] BS: $BaSiO_3$; BB_2: BaB_2O_4; BS_2: $BaSi_2O_5$; H: hexacelsian ($BaAl_2Si_2O_8$); G: glass.
[b] Those samples have abnormal expansion between 120 and 150 °C due to the presence of $BaSiO_3$ phase in the glasses. The CTE value was measured between 200 and 550 °C.

2.3. Thermal mechanical analysis (TMA)

Bulky glass samples with a length of 5 mm and a cross-section area of 40 mm^2 were tested under a load of 1 N, applied with an Al_2O_3 push rod. The heating rate used in expansion measurements was 10 °C/min. Thermal expansion and dilatometric softening temperature (T_s) were measured on green glass pellets or annealed cylindrical glasses using a thermal mechanical analyzer (TMA 2940, TA, DuPont, USA) and pushrod dilatometer (NETZSCH DIL 402C). The softening temperature (T_s) of a glass is defined by finding a turning point of shrinkage when heated under a constant load.[34] Before the measurement, the glasses were annealed at $T_g + 10$ °C for 1 h to relax the residual thermal stress. In order to get reliable and high quality expansion data, the data of the first run for each sample was disregarded due to the uneven contact of the sample with the push rod. To avoid this effect, the sample was pre-treated by heating and cooling from below the T_g point to 200 °C above it for 2–3 cycles, until the heating curves were reproducible.

2.4. Microstructural observations and elemental analysis

The sample was polished and cleaned in an ultrasonic bath of ethanol solution for at least a few cycles. A thin layer of carbon was then coated on the surface to improve its electrical conductivity. The morphologies of polished surfaces or cross-sections of the samples were analyzed using a field-emission scanning electron microscope (SEM, Leo Instrument 1530, England) equipped with an X-ray energy dispersive spectrometer (EDS, DX-4, EDAX Co., USA), and electron probe microscopic analysis (EPMA, JXA-8200, JEOL, Japan). The signal collection for the EDS and EPMA-WDS line scan of Ce was set to detect the signals from Ce *M-orbit*, rather than Ce *L-orbit* because one peak of the Ce L_α*-orbit* (4.839 keV) signal nearly overlapped with Ba L_β (4.827 keV).

2.5. Wetting and compatibility test

The substrates for wetting and long-term tests were made from 8 mol% Y_2O_3-doped ZrO_2 (8YSZ), 20 mol% $SmO_{1.5}$-doped CeO_2 (20SDC), Crofer 22 APU, or YSZ/NiO (60/40 volume ratio) composite. The dense 8YSZ and 20SDC disks were prepared via the following steps. First, 1.2 g of YSZ powder (TEAMCera, Taiwan) or SDC powder (made by an in-house co-precipitation method) was die-pressed, and held at a pressure of 66.0 MPa for 60 s. The disks were then sintered at 1500 °C for 1 h to obtain dense ceramic disks. YSZ/NiO composite anode substrates were prepared using a tape casting method.[8] Crofer 22 APU (abb. as "Crofer", manufactured by Tyssen Krupp, Germany) is a ferritic stainless steel containing 22 wt% Cr, and has a CTE vale of 11.8 ppm/K.[12,17] Cracking due to crystallization within the glasses or the mismatch of its CTE with substrates was also investigated to assess the material compatibility. To measure the wetting of materials, a 6 mm diameter and 4 mm thick green disk (un-sintered) was put on a specified substrate. The substrate and disk were heated at 10 °C/min. An optical instrument (Nabatherm, model HT 04/17 s, Germany) with two cameras was used to directly observe an image projection of the molten sample. A detailed description of this method can be found in our previous work.[16] A long-term test was also conducted in a reducing atmosphere. The furnace was ventilated with a mixture of pure H_2/H_2O gas, which had been passed

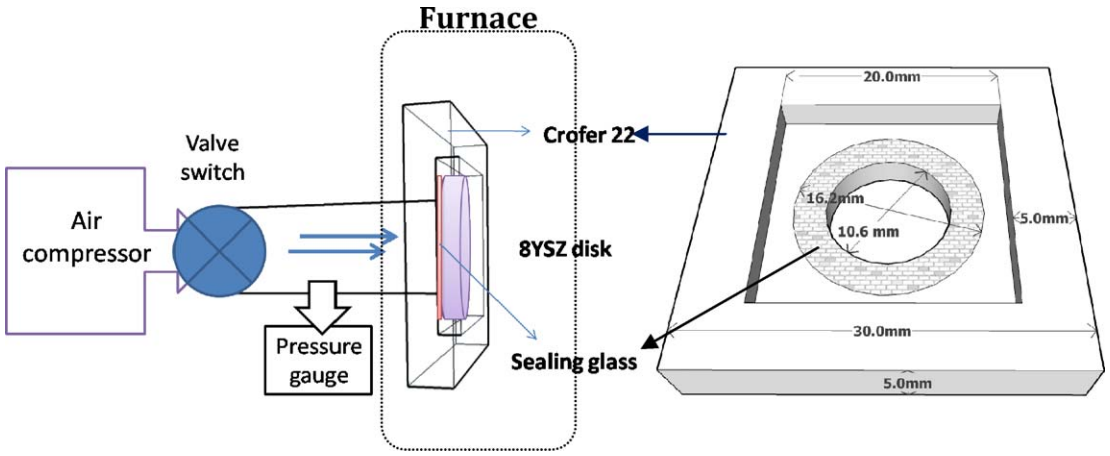

Fig. 1. Schematic diagram of the leakage testing apparatus and detailed dimensions of the testing tools.

through de-ionized water at 25 °C. The furnace atmosphere due to this flow is equivalent to 97% H_2–3% H_2O.[1]

2.6. Leakage test

The test on G6 glass was performed at either room temperature or 650 °C. An 8YSZ disk (sintered at 1500 °C for 1 h, fully dense with a 16.2 mm diameter and 3.0 mm thickness) was sealed on a Crofer sample holder (Fig. 1) using G6 glass. The pressurized gas was supplied by an air compressor. The surface area of the cell was 30 mm × 30 mm. Details of the testing apparatus are shown in Fig. 1. The leakage rate (L) was calculated using the following equation[37,38]:

$$L = \frac{V_m \times 0.987(P_i - P_f)V}{\Delta t \times R \times T \times C}\ \text{sccm cm}^{-1}, \quad (2)$$

where V_m is the molar volume of an ideal gas (22414 cm^3), P_i is the initial pressure, P_f is the final pressure, V is the internal volume of the gas reservoir and the pipe, Δt is the elapsed time as the pressure decreased from P_i to P_f, R is the universal gas constant (0.08206 l m K^{-1} mol^{-1}), T is the testing temperature, and C is the peripheral length of the glass seal. In this study, $P_i - P_f$ was maintained at 0.2 bar, V is 131.0 cm^3, and C is 50.8 cm. Before testing, the background leakage of the equipment at room temperature and 650 °C was determined and used to calibrate the measurements.

[1] The saturated water vapor pressure at 25 °C is 23.76 mm Hg, equivalent to 0.0031 atm.[35] The equilibrium pressure of each gaseous species can be obtained from the following equation[36]:

$$\Delta G^0 = -247,500 + 55.87T(J) = -RT \ln\left(\frac{P_{H_2O}}{P_{O_2^{1/2}} \cdot P_{H_2}}\right)$$

Therefore:

$$\log P_{O_2} = 2\log\left(\frac{P_{H_2O}}{P_{H_2}}\right) + 4.84 - 2852.4 \times \frac{1}{T},$$

where P_{H_2} was set at 1.0 atm, P_{H_2O} is 0.0031 atm, and T is 923 K (650 °C).

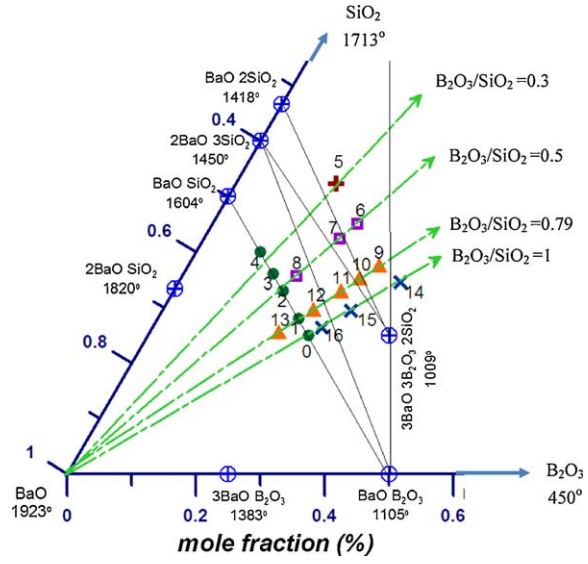

Fig. 2. Phase diagram of the BaO–B_2O_3–SiO_2 ternary system and the formulations of indicated G-series (G0–G16) glasses.

3. Results and discussion

3.1. Synthesis and characterization of G-series glasses

All formulations (except G1A5 and G1A10) of the glass systems are plotted in the BaO–SiO_2–B_2O_3 ternary phase diagram shown in Fig. 2. G0 and G1, which had higher B_2O_3/SiO_2 ratios (≥0.79) and were water-quenched from the molten state, formed a glassy (amorphous) state. A $BaSiO_3$ crystalline phase was observed in the water-quenched samples of G2 and G3. On the other hand, water-quenched G4, which has a lower B_2O_3/SiO_2 ratio (0.25), had several diffraction peaks that were matched to $BaSiO_3$ and $BaSi_2O_5$ phases. Hence, $B_2O_3/SiO_2 = 0.50$ is at the amorphous/crystalline boundary for this system. B_2O_3, when is used as a glass former, tends to increase the fluidity of glass. An increase in B_2O_3 content lowers the melting point and helps to stabilize the amorphous phase.

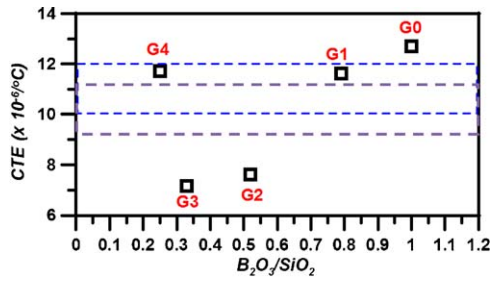

Fig. 3. CTE of several G-series glasses as a function of the B_2O_3/SiO_2 ratio in the BaO–SiO_2–B_2O_3 glass system. G3 and G4 are glass-ceramics not pure glasses. The CTE of G3 and G4 are shown for reference only.

3.1.1. Effect of B_2O_3/SiO_2 on CTE

Fig. 3 shows the CTE as a function of B_2O_3/SiO_2 ratio in BaO–SiO_2–B_2O_3 glass systems. Normally, the overall CTE increases as SiO_2 content decreases (B_2O_3 increases) because of the low CTE of pure SiO_2 (0.6 ppm/K) and high CTE of B_2O_3 (14.4 ppm/K). The other reason for the CTE change with B_2O_3 content is consistent with previous reports.[23,24,28,29,34] The G2, G3 and G4 samples are glass ceramics. $BaSiO_3$ and/or $BaSi_2O_5$ crystals formed after quenching in water. The different CTE of $BaSiO_3$ and $BaSi_2O_5$ phases (9–13 and 14 ppm/K, respectively[4]) and the quantity of the crystalline phases also contribute to the CTE value of these glass-ceramics.

Crystal growth in the G0 glass sample after aging at 850 °C for 10 h was investigated. Two phases, $BaSiO_3$ and BaB_2O_4, were found in the G0 glass. This result was consistent with the information presented in the phase diagram (Fig. 2). The microstructure of the heat-treated G0 glass-ceramic contained several fine cracks across the $BaSiO_3$ grains. These cracks are possibly due to a mismatch in the CTE of the glass matrix and the crystalline phases. Differential thermal contraction may have induced tensile stresses, and led to cracking in the grains. The similar phenomenon can be observed in the cases of G0, G2, G3 and G4. Therefore, G0, G2, G3 and G4 were not selected as candidates for further testing of suitable seals.

3.1.2. Thermal properties and GFA evaluation

DTA results for the glasses (G0 and G1 with Al_2O_3), including the thermal properties, T_g, T_c, and T_l are summarized in Table 2. As the content of B_2O_3 increases, the glass transition temperature, the softening temperature, and T_l decrease. T_g values of G1, G1A5 and G1A10 glasses are in a range close to the lower operation temperature (550 °C) of IT-SOFC. Here in the table, T_{c1} and T_{c2} represent the $BaSiO_3$ and $BaAl_2Si_2O_8$ formation temperature of those G1 to G4 glass systems, respectively.

Determination and/or evaluation of the glass-forming tendency have attracted much attention in the past five decades. Among the available evaluation methods, the simplest one is the reduced glass transition temperature, T_{rg}, proposed by Kauzmann,[20] who has investigated several glass systems and established a criterion for a good glass-forming tendency

$$T_{rg} \geq \frac{2}{3}\left(\frac{T_g}{T_l}\right). \quad (3)$$

However, the T_{rg} values of G0, G1 and G1A5 in Table 2 are larger than 0.66. Therefore, this criterion does not reflect good GFA for the tested glasses.

The other GFA parameters, relative glass-forming tendency (τ_g) and glass stability or resistance to crystallization on heating (K_H) have also been reported in the literature.[21,22] The G-glasses had similar values for these GFA parameters, except the K_H of G1. Consideration of the GFA and CTE (Fig. 3) suggests that G1 glass seems to be the best among G0 to G4. However, Fergus[25] pointed out that the above parameters are not absolute indicators of GFA. Instead, they are scanning-rate-dependent parameters. In order to prevent instant crystallization after glass

Table 2
Thermal properties of developed G glasses.

Glass No.	T_g (°C)	T_x (°C)	T_{c1}[a] (°C)	T_{c2}[a] (°C)	T_s (°C)	T_l (°C)	T_{rg}[b]	τ_g[b]	K_H[b]	γ[b]
G0	545	609	674	716	600	887	0.71	0.16	0.23	0.446
G1	553	634	674	702	700	918	0.69	0.15	0.29	0.450
G1A5	547	676	694	735	605	863	0.72	0.18	0.69	0.485
G1A10	563	699	729	806	590	1168	0.58	0.20	0.29	0.427

[a] T_{c1} and T_{c2} are crystallization temperature of $BaSiO_3$ (BS) and BaB_2O_4 (BB2) for G0 glass, BS and hexacelsian ($BaAl_2Si_2O_8$) for G1, G1A5 and G1A10 glasses.
[b] The definition of the parameters γ and T_{rg} is shown in text. The others are $\tau_g = (T_c - T_g)/T_g$, $K_H = (T_x - T_g)/(T_l - T_x)$.

Table 3
Quantitative analysis results of laboratory or mass produced-G6 glass.

Mol%	Starting composition (mol%)	Produced in lab.		Produced by ExoJet	
		EDS[a]	Calibrated[c]	EDS[a]	Calibrated[c]
Al_2O_3	0.00	1.70	1.32	4.90	3.80
SiO_2	45.06	57.20	44.48[b]	58.20	45.08[b]
BaO	32.40	41.10	31.96	36.90	28.58
B_2O_3	22.54	N/A	22.24[b]	N/A	22.54[b]

[a] The value of molar percentage is the average of 5 random selected points by EDS analysis. All EDS results were calibrated by standard sample.
[b] Molar content of B_2O_3 was calculated according to the ratio $B_2O_3/SiO_2 = 0.5$.
[c] Molar percentages of those four compositions were calibrated based on the EDS results and selected B_2O_3/SiO_2 ratio.

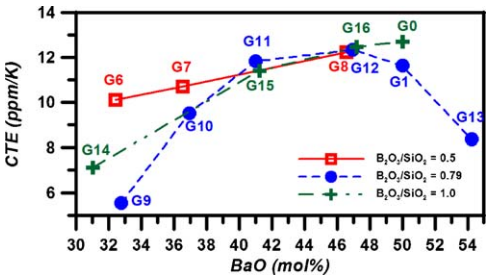

Fig. 4. CTE of G-series glasses as a function of BaO content in $BaO–SiO_2–B_2O_3$ glasses with different B_2O_3/SiO_2 ratios.

synthesis (un-favored $BaSiO_3$ (BS) phase formation), G1 glass was selected as the next target for studying the effect of Al_2O_3 addition because instant crystallization after glass synthesis was less likely with this oxide.

3.1.3. *Effect of Al_2O_3 addition on CTE*

Al^{3+} can be a network former (as a tetrahedral AlO_4 group) or modifier (as an octahedral AlO_6 group) depending on the content of Al_2O_3 in a glass formulation. When the Al ion is tetrahedrally coordinated, small amounts of Al^{3+} play the role of a network former and enhance the glass structure symmetry. However, when the coordination number changes to six, it acts as a modifier.[19] The CTE values of G1A5 and G1A10 decrease with increasing Al_2O_3 content. Another possible reason for a change in CTE values of the synthesized samples is the formation of crystalline phase in glass. A crystalline phase that may form in $BaO–SiO_2–B_2O_3–Al_2O_3$ quaternary systems is polymorphous $BaAl_2SiO_8$, having hexacelsian, monocelsian, and orthocelsian structures. Their CTE values are 7–8, 2–3 and 5–7 ppm/K,[4] respectively. After introducing Al_2O_3 in the formula of G1A5 and G1A10, two crystals, $BaSiO_3$ and $BaAl_2Si_2O_8$ (hexacelsian and monocelsian), were detected after long-term aging at 800–850 °C in both G1A5 and G1A10 glasses.

3.1.4. *Effect of BaO addition on CTE*

The previous results sparked investigation of additional glass formulae. G5–G16 glasses were prepared to find a suitable glass with a CTE in an acceptable range, and also maintained a non-crystalline state after long-term heat treatment. Fig. 4 shows several CTE results as a function of BaO content in the $BaO–SiO_2–B_2O_3$ glass system (no Al_2O_3) at different B_2O_3/SiO_2 ratios.

BaO plays a role of network modifier in the glass system and results in non-bridging oxygen species. Therefore, the CTE increases with the BaO content. Similar results were obtained in $BaO–Al_2O_3–La_2O_3–B_2O_3–SiO_2$ systems reported by Sohn et al.[23] Fergus[25] reported that the CTE of $BaO–MgO–SiO_2$ and $BaO–ZnO–SiO_2$ systems might increase with increasing BaO content due to the formation of barium silicate, $BaSiO_3$. A similar viewpoint has also been mentioned by Goel et al.[28,30] One exception to the trend, G13, is probably due to a change in the role of BaO, which induces the formation of $BaSiO_3$ and/or other BaO-crystalline phases. The G13 is a glass ceramic and has a lower CTE than those of G11 and G12.

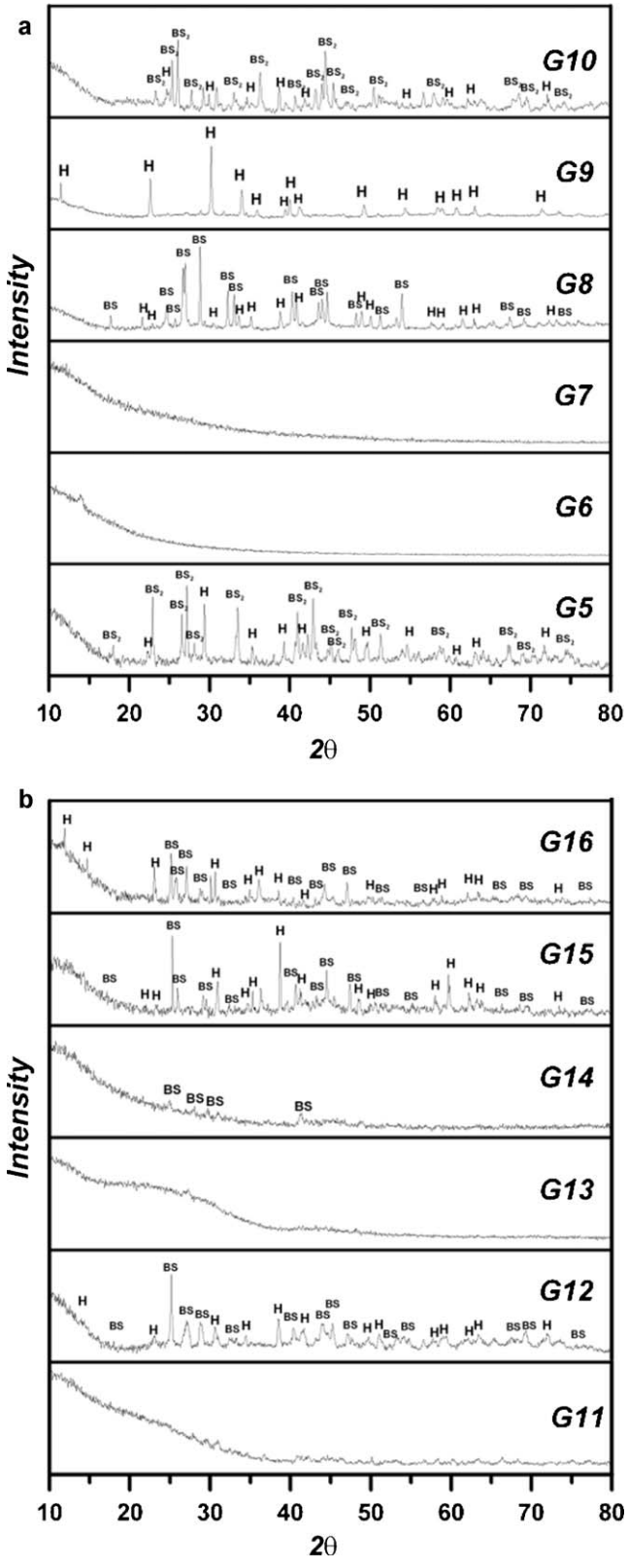

Fig. 5. XRD patterns of (a) G5–G10 and (b) G11–G16 glass-ceramics heat-treated at 850 °C for 100 h.

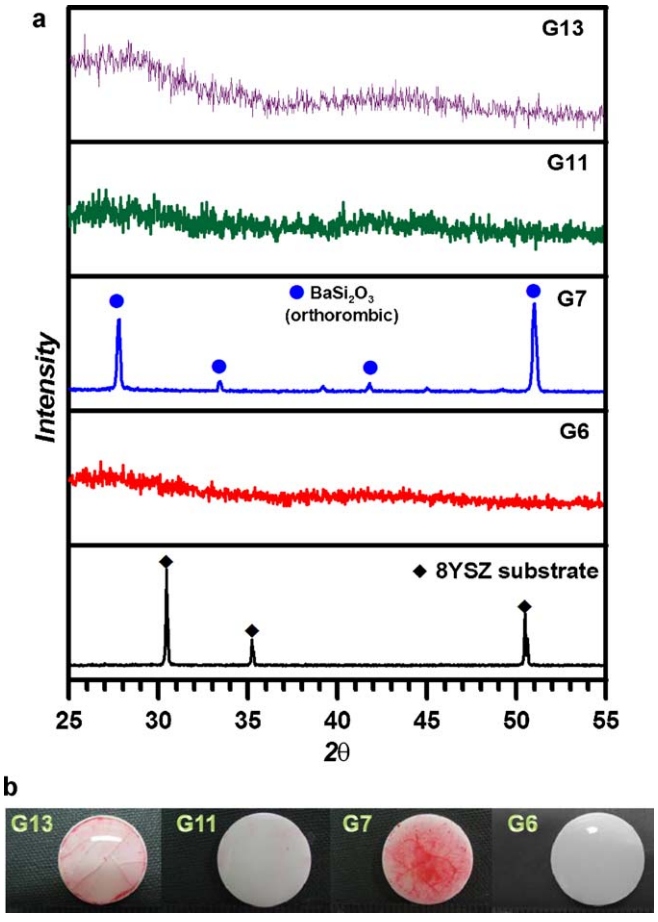

Fig. 6. (a) XRD patterns of 8YSZ substrate and G6, G7, G11 and G13 glasses melted onto 8YSZ at 1100 °C and cooled in the furnace. (b) Photo images of these four glasses on 8YSZ substrate show that fine cracks are present in G13 and G7. The cracks are apparent because of the application of red dye.

3.1.5. Effect of thermal-treatment on crystallization behavior

G5–G16 samples, which were quenched into de-ionized water after melting in the furnace at 1300 °C for 30 min, only showed amorphous phases that were detected by XRD. All of the samples remained amorphous even after heat-treatment at 650 °C for 100 h. However, some crystalline phases, such as $BaSi_2O_5$ (abbreviated as BS2), Ba_2SiO_4 (B2S) or $BaAl_2Si_2O_8$ (H) of the glasses were detected by XRD in G5, G8–10, G12 and G14–16 after being heat-treated at 750 °C for 100 h. G6, G7, G11 and G13 remained amorphous even after heat-treatment at 850 °C for 100 h (Fig. 5). Therefore, these four glasses were chosen for the following wetting tests.

Green G6, G7, G11 and G13 glass pellets were made by die-pressing. The pellets measured 6.0 mm in diameter and 1.2 mm thick were placed on a 8YSZ disk, then melted at 1100 °C for 15 min and cooled in the furnace. XRD results (Fig. 6(a)) show that a crystalline $BaSi_2O_3$ phase is formed in the G7/YSZ sample. Moreover, some cracks could be seen in G7 and G13 (Fig. 6(b)). Therefore, G6 and G11 were considered as the best candidates for further sealing tests.

The thermal expansion properties of G6 and G11 had been measured and the CTE of the glasses were 10.2 ppm/K and 11.7 ppm/K, respectively. Both glasses were used as sealant of thin YSZ plate (about 100 μm) on Crofer fixture, as shown in Fig. 1. Only the case sealed with G6 glass had no defects (e.g., fine cracks) after several thermal cycles between room and 650 °C. G6 was the last and the best sealing glass among 17 glasses and was selected as the glass for the following sealing tests in this study.

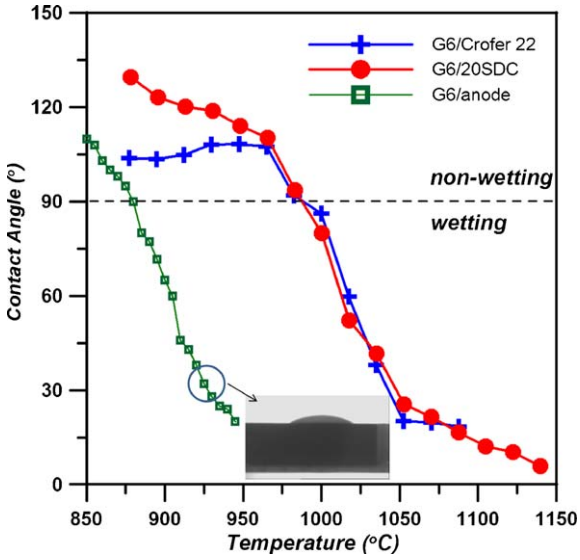

Fig. 7. Contact angle of M-G6 glass green pellet melted on 20SDC, Crofer and NiO/YSZ anode substrates as a function of temperature. Samples were heated at a rate of 10 K/min.

3.2. Sealing properties of G6 glass

To ensure that mass-produced G6 (M-G6) glass performed equally well as the G6 made in the laboratory, M-G6 samples were tested as before. They performed similarly to the G6 glass samples. A detailed comparison of the G6 glass samples from different sources is shown in Table 3. The M-G6 glass features Al_2O_3 contamination that originated from the melting crucible. An additional 2.5 mol% Al_2O_3 is present in this glass as a result.

3.2.1. Wetting behavior of G6

Fig. 7 shows the wetting behavior of a M-G6 glass pellet melted at a heating rate of 10 °C/min on SDC, Crofer, and anode substrates as a function of the temperature M-G6 was able to wet all substrates at temperatures greater than 970 °C. Therefore, 1000 °C was selected as the sealing temperature in the following tests.

3.2.2. Stability of long-term tests

Layered 20SDC/M-G6/8YSZ samples were subjected up to 5000 h long-term tests in air. No cracks or secondary phases were observed and elemental mapping results showed that no inter-diffusion of elements had occurred after 2000 h heat treatment (the data is not shown here). Extending to 5000 h test, still no cracks but secondary phases were observed at the interface. In order to improve the accuracy of the results, an EPMA-WDS line scan across the interface of G6/8YSZ and G6/20SDC was

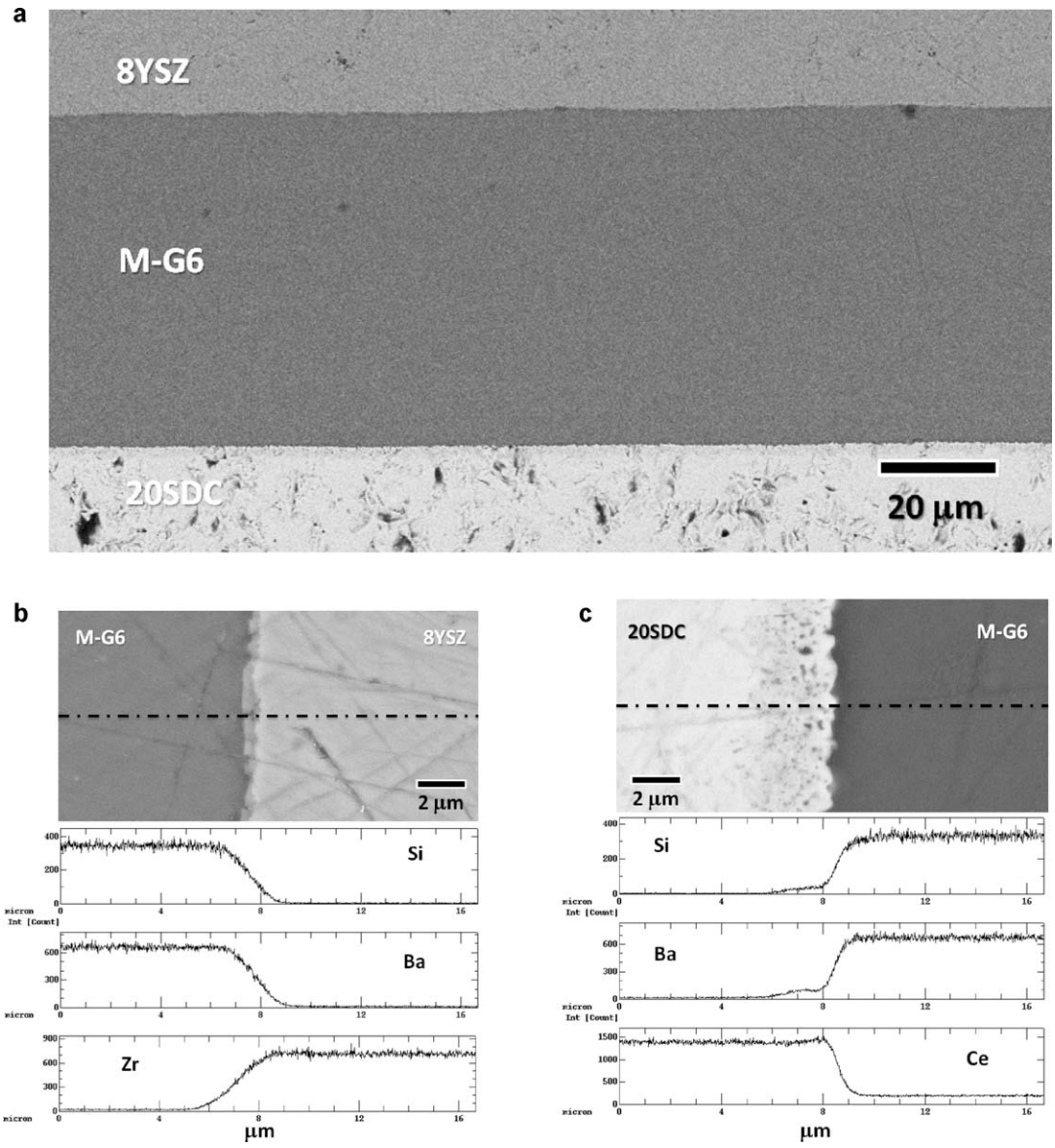

Fig. 8. (a) SEM image (low magnification) of 20SDC/M-G6/8YSZ samples aged at 650 °C for 5000 h after sealing at 1000 °C for 30 min in air. The enlarged BSE image and WDS line profiles of elemental composition at the interfaces of (b) M-G6/8YSZ and (c) M-G6/20SDC.

executed. The beam size of the WDS was about 1 μm. Therefore, the diffusion region located at the interface and measuring more than 2 μm can be considered to contain the reaction layer. Fig. 8(b) shows that a sub-micron thick layer formed which contains Si and Ba. Additional Zr element slightly diffused into the G6 sealing glass with a diffusion distance less than 1 μm. The secondary phase shown at the interface in Fig. 8(b-1) is possibly (Ba,Zr)SiO_3, which could be formed due to the presence of ZrO_2.

Similar analysis was also accomplished for the G6/20SDC interface. No new crystalline phases could be observed, but glass penetration into the surface of 20SDC was evident, as shown in Fig. 8(c). The penetration depth of Si and Ba elements is about 2 μm. Diffusion of Ce into the G6 was not apparent.

Planar SOFC often utilize an anode-support structure, since a thinner electrolyte layer on the anode yields better performance due to a lower resistance.[8–10] The interfaces between M-G6 and the anode and Crofer were therefore investigated. Fig. 9 shows that there was good bonding at the G6/anode and G6/Crofer interfaces. No cracks, delamination, or secondary phases were observed after 5000 h annealing. Additionally, no inter-diffusion of the constituent elements was observed at low magnification.

Smeacetto et al.[38] used a different sealing glass (containing SiO_2, Al_2O_3, CaO, and Na_2O ingredients) to join Crofer and YSZ. Some crystalline phases were observed in their glass system. They reported that the pre-oxidized treatment of Crofer 22 at 950 °C in air for 2 h could form a Cr_2O_3 barrier layer, and prevent Cr ions from diffusing into the sealing layer. Fig. 9(b-2) shows that in this study, Cr enrichment was detected on pre-oxidized Crofer and aged G6/Crofer samples. Yang et al.[39] also reported that it is possible to form $BaCrO_4$ via the reaction of Ba–Ca–Al–Si–B–oxide glass with chromia-based alloy, i.e., AISI446, FeCr alloy and Crofer 6025HT if treated in air at 850 °C for 1 h, followed by 750 °C for 4 h. The formation

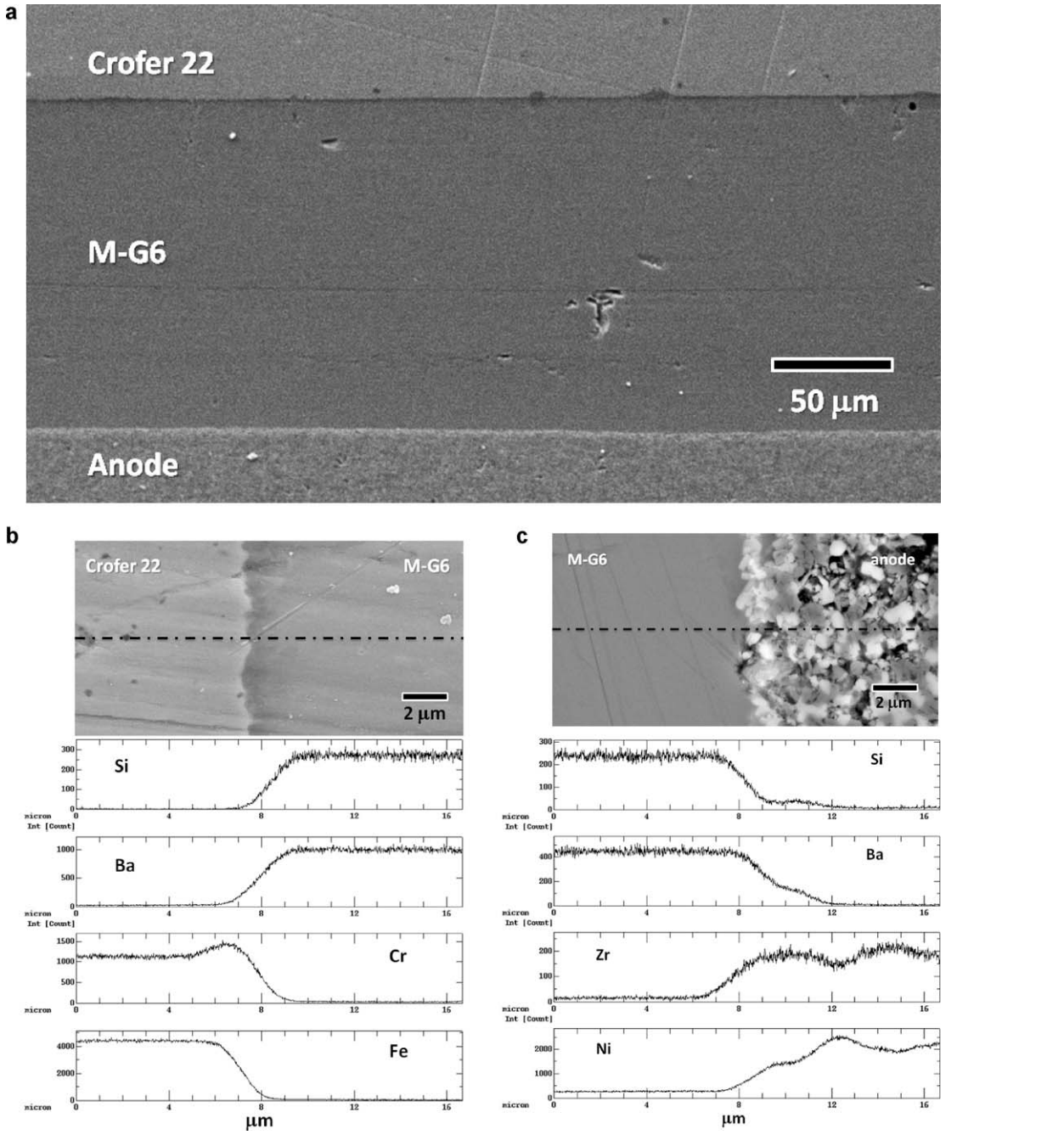

Fig. 9. (a) SEM-BSE image (low magnification) of Crofer 22/M-G6/anode sample aged at 650 °C for 5000 h after sealing at 1000 °C for 30 min in air. The enlarged BSE image and WDS line profiles of elemental composition at the interface of (b) M-G6/Crofer 22 and (c) M-G6/anode.

of $BaCrO_4$ leads to the depletion of Ba in the glass system, and possibly results in the delamination of chromia-forming alloy from the glass due to a mismatch in CTE. At the interface of M-G6/Crofer, the formation of $BaCrO_4$ in the 5000 h annealed sample was not apparent. Results of a EPMA-WDS line scan across the interface of Crofer/M-G6 show a Cr-rich layer in a thickness of 2 μm (Fig. 9(b-2)), implying that a spinel $Ba(Cr,Fe)_2O_4$ is possibly formed, which is similar to a Cr–Mn–spinel phase mentioned by Smeacetto et al.[38]

The microstructure at the M-G6/anode interface (Fig. 9(c-1)) shows that the Ba and Si elements of the glass clearly penetrate into the anode layer to about a 4 μm depth. Fig. 9(c-2) indicates that this is partly due to the porous structure of the anode. Similarly, a small amount of the Zr from the anode diffused into the glass region about 2 μm deep. There are no noticeable secondary phases formed near the interface even after 5000 h of heat treatment.

3.2.3. Stability test in reduction atmosphere

The SOFC anode is always exposed to a strong reducing atmosphere with pure H_2 or another fuel gas during operation. The M-G6/anode was therefore analyzed at 650 °C in a reduc-

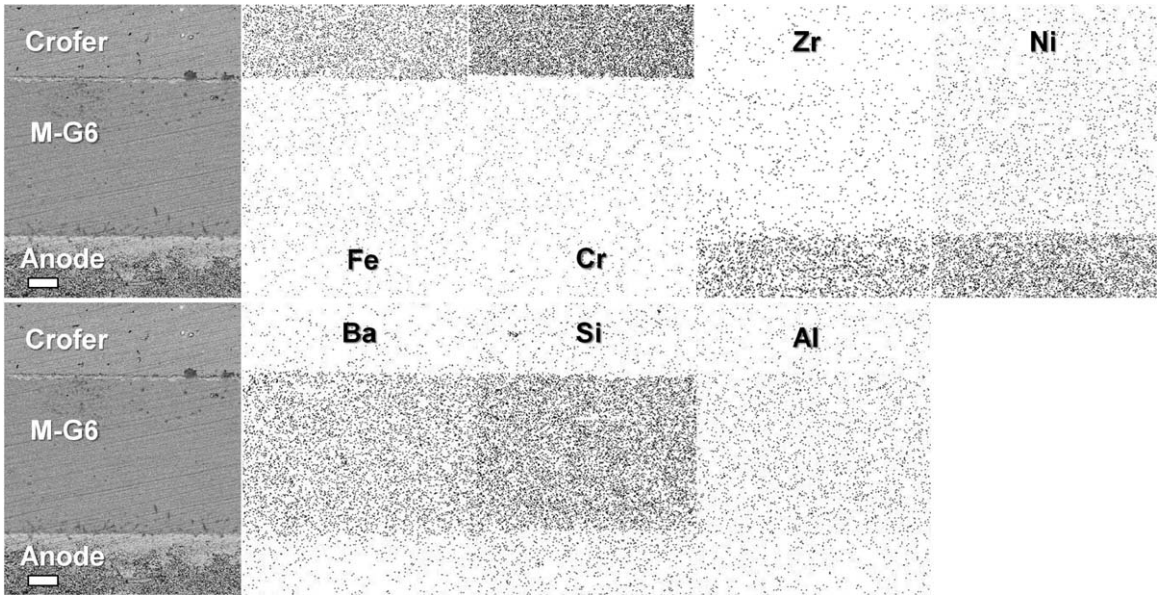

Fig. 10. Elemental mapping of a Crofer/M-G6/anode annealed at 650 °C for 20 h in a reducing atmosphere (pure H_2 gas flow passed through 25 °C de-ionized water) after sealing at 1000 °C for 30 min in air.

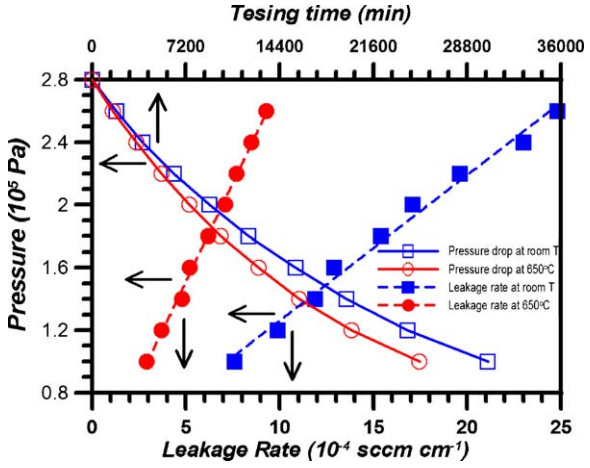

Fig. 11. Leakage tests results of a 8YSZ disc-Crofer 22 testing kit sealed using M-G6. The testing conditions were 2.8×10^5 Pa to 1.0×10^5 Pa at room temperature and 650 °C, respectively. The duration of testing was about 20 days.

ing atmosphere. The partial pressure of oxygen in equilibrium was 10–26 atm, similar to the conditions reported by Smeacetto et al.[38] Fig. 10 shows the results at the interface in the G6/anode. The anode is clean in low-magnification condition and no additional phases appear under reducing conditions. Similarly, no apparent inter-diffusion of the elements was observed.

3.2.4. Leakage test

A leakage test of an 8YSZ-Crofer testing fixture sealed by M-G6 was conducted under air pressures ranging from 280 kPa to 100 kPa (pressure difference from atmosphere) at room temperature and 650 °C, respectively. The results are shown in Fig. 11. At room temperature the leakage rate was 8×10^{-4} sccm cm^{-1} and 25×10^{-4} sccm cm^{-1} at a pressure of 100 kPa and 260 kPa, respectively. While testing at 650 °C, the leakage rate was 3×10^{-4} sccm cm^{-1} and 9×10^{-4} sccm cm^{-1} at pressures of 100 kPa and 260 kPa, respectively. It took approximately 20 days for the pressure to fall from 280 kPa to about 100 kPa. The pressure conditions used in this study were higher than those reported in the literature,[37,40–42] which tested below 20 kPa and observed a leakage rate through the glass-ceramic sealant on the order of 10^{-4} sccm cm^{-1}.[41] Among all the leakage tests, the result of compressive sealant by Chou and Stevenson[41] has the best record of 10^{-2} sccm cm^{-1}; however, this was measured at 800 °C.

4. Conclusions

The effects of B_2O_3/SiO_2, Al_2O_3 and BaO contents on the CTE of G-series glasses have been investigated. Among the 19 G-series glasses, G6 had an appropriate CTE, good wetting characteristics, and excellent interface stability with electrolytes, anode, and Crofer. The glass wets very well on 8YSZ, 20SDC, Crofer, and NiO/YSZ, and is able to seal the substrates at 1000 °C. No cracks, substantial secondary or crystalline phases of the M-G6 glass sealing were detected by SEM, elemental mapping, EPMA and XRD after heat treatment for as long as 5000 h. However, thin reaction layers of about 2 μm thickness were identified at the interfaces of M-G6/8YSZ and M-G6/Crofer after 5000 h annealing tests. The diffusion of M-G6 glass into the anode surface and the diffusion of Zr elements from YSZ into M-G6 are possibly responsible for producing a 4 μm diffusion layer after the 5000 h test. Good bonding was sustained even after the long-term tests. The interfaces of G6/YSZ, G6/SDC, G6/Crofer, and M-G6/anode remained intact. At 650 °C and 100 kPa, M-G6 glass had a leakage rate of 3×10^{-4} sccm cm^{-1}. Even when the pressure was elevated to 260 kPa, the leakage rate was only 9×10^{-4} sccm cm^{-1}. This led

to the conclusion that M-G6 glass is potentially a good sealing material for IT-SOFCs.

Acknowledgment

The authors thank the National Science Council in Taiwan (NSC96-2221-E-002-027-MY2 and NSC97-2221-E-002-027-MY2) for funding support and helpful comments for paper reviewers.

References

1. Minh NQ. Ceramic fuel cell. *J Am Ceram Soc* 1993;**76**(3):563–88.
2. Blum L, Meulenberg WA, Nabielek H, Wilckens RS. Worldwide SOFC technology overview and benchmark. *Int J Appl Ceram Technol* 2005;**2**(6):482–92.
3. Molenda J, Świerczek K, Zając W. Functional materials for the IT-SOFC. *J Power Sources* 2007;**173**:657–70.
4. Fergus JW. Electrolyte for solid oxide fuel cells. *J Power Sources* 2006;**162**:30–40.
5. Esposito V, Traversa E. Design of electroceramics for solid oxide fuel cell application: playing with ceria. *J Am Ceram Soc* 2008;**91**(4):1037–51.
6. Liu Y, Hashimoto S, Nishino H, Takei K, Mori M. Fabrication and characterization of a co-fired $La_{0.6}Sr_{0.4}Co_{0.2}Fe_{0.8}O_{3-\delta}$ cathode-supported $Ce_{0.9}Gd_{0.1}O_{1.95}$ thin-film for IT-SOFCs. *J Power Sources* 2007;**164**:56–64.
7. Ding X, Cui C, Du X, Guo L. Electrical conductivity, thermal expansion and electrochemical properties of Fe-doped $La_{0.7}Sr_{0.3}CuO_{3-\delta}$ cathodes for solid oxide fuel cells. *J Alloys Compd* 2009;**475**:418–21.
8. Chen YY, Wei WCJ. Processing and characterization of ultra-thin yttria-stabilized zirconia (YSZ) electrolytic films for SOFC. *Solid State Ionics* 2006;**177**:351–7.
9. Corbin SF, Clemmer RMC, Yang Q. Development and characterization of porous composites for solid oxide fuel cell anode conduction layers using ceramic-filled highly porous Ni foam. *J Am Ceram Soc* 2009;**92**(2):331–7.
10. Hagen A, Barfod R, Hendriksen PV, Liu YL, Ramousse S. Degradation of anode supported SOFCs as a function of temperature and current load. *J Electrochem Soc* 2006;**153**(16):1165–71.
11. Hui S, Yang D, Wang Z, Yick S, Decès-Petit C, Qu W, et al. Metal-supported solid oxide fuel cell operated at 400–600 °C. *J Power Sources* 2007;**167**:336–9.
12. Zhu JH, Geng SJ, Ballard DA. Evaluation of several low thermal expansion Fe–Co–Ni alloys as interconnect for reduced-temperature solid oxide fuel cell. *Int J Hydrogen Energy* 2007;**32**:3682–8.
13. Mahapatra MK, Lu K. Glass-based seals for solid oxide fuel and electrolyzer cells—a review. *Mater Sci Eng R* 2010;**67**:65–85.
14. Bansal NP, Gambleet EA. Crystallization kinetics of a solid oxide fuel cell seal glass by differential thermal analysis. *J Power Sources* 2005;**147**:107–15.
15. Haanappel VAC, Shemet V, Gross SM, Koppitz T, Menzler NH, Zahid M, et al. Behavior of various glass-ceramic sealants with ferritic steels under simulated SOFC stack conditions. *J Power Sources* 2005;**150**:86–100.
16. Chen CL, Wei WCJ, Roosen A. Wetting, densification and phase transformation of $La_2O_3/Al_2O_3/B_2O_3$-based glass-ceramics. *J Eur Ceram Soc* 2006;**26**:59–65.
17. Smeacetto F, Salvo M, Ferraris M, Cho J, Boccaccini AR. Glass-ceramic seal to join crofer 22 APU alloy to YSZ ceramic in planar SOFCs. *J Eur Ceram Soc* 2008;**28**:61–8.
18. Wei WCJ. Sealing glass-ceramics for solid oxide fuel cell. *Recent Patents Mater Sci* 2008;**1**:218–22.
19. Lu ZP, Liu CT. Glass formation criterion for various glass-forming systems. *Phys Rev Lett* 2003;**91**:115505.
20. Kauzmann W. The nature of the glassy state and the behavior of liquids at low temperatures. *Chem Rev* 1948;**43**:219–56.
21. Ouchetto M, Elouadi B, Parke S. Infrared investigation of chemical durability of lanthanum–zinc ultra-phosphate glasses. *Phys Chem Glasses* 1991;**32**(2):43–7.
22. Hrubý A. Evaluation of glass-forming tendency by means of DTA. *Czech J Phys* 1972;**22**:1187–93.
23. Sohn SB, Choi SY, Kim GH, Song HS, Kim GD. Stable sealing glass for planar solid oxide fuel cell. *J Non-Cryst Solids* 2002;**297**:103–12.
24. Sohn SB, Choi SY, Kim GH, Song HS, Kim GD. Suitable glass-ceramic sealant for planar solid-oxide fuel cells. *J Am Ceram Soc* 2004;**87**(2):254–60.
25. Fergus JW. Sealants for solid oxide fuel cells. *J Power Sources* 2005;**147**:46–57.
26. Chou YS, Stevenson JW, Singh P. Novel refractory alkaline earth silicate sealing glasses for planar solid oxide fuel cells. *J Electrochem Soc* 2007;**154**(7):B644–51.
27. Wang R, Lü Z, Liu C, Zhu R, Hung X, Wei B, et al. Characteristics of a SiO_2–B_2O_3–Al_2O_3–$BaCO_3$–PbO_2–ZnO glass-ceramic sealant for SOFCs. *J Alloys Compd* 2007;**432**:189–93.
28. Goel A, Tulyaganov DU, Kharton VV, Yaremchenko AA, Eriksson S, Ferreira JMF. Optimization of La_2O_3-containing diopside based glass-ceramic sealants for fuel cell applications. *J Power Sources* 2009;**189**:1032–43.
29. Goel A, Tulyaganov DU, Pascual MJ, Shaaban, Muñoz ERF, Lü Z, et al. Development and performance of diopside based glass-ceramic sealants for solid oxide fuel cells. *J Non-Cryst Solids* 2010;**356**:1070–80.
30. Goel A, Tulyaganov DU, Kharton VV, Yaremchenko AA, Eriksson S, Ferreira JMF. Optimization of La_2O_3-containing diopside based glass-ceramic sealants for fuel application. *J Power Sources* 2009;**189**:1032–43.
31. Ojovan MI, Lee WE. *An introduction to nuclear waste immobilization*. UK: Elsevier Science, Ltd.; 2009. ISBN:978-0-08-044462-8 [Chapter 17].
32. Shelby JE. *Introduction to glass science and technology*. Cambridge, UK: ISBN, The Royal Soc. Chem.; 2005 [Chapter 7].
33. Lin SE, Chen YR, Wei WCJ, Hsueh CH. BaO–B_2O_3–SiO_2–Al_2O_3 sealing glass for intermediate temperature solid oxide fuel cell. *J. Non-Cryst. Solids*; submitted for publication.
34. Mahapatra MK, Lu K, Bodnar RJ. Network structure and thermal property of a novel high temperature seal glass. *Appl Phys A* 2009;**95**:493–500.
35. http://www.mwit.ac.th/~physicslab/hbase/kinetic/watvap.html.
36. Turkdogan ET. *Physical chemistry of high temperature technology*. New York: Academic Press; 1980. p. 5–24.
37. Zhang T, Zhu Q, Xie Z. Modeling of cracking of the glass-based seals for solid oxide fuel cell. *J Power Sources* 2009;**188**:177–83.
38. Smeacetto F, Chrysanthou A, Salvo M, Zhang Z, Ferraris M. Performance and testing of glass-ceramic sealant used to join anode-supported-electrolyte to Crofer 22 APU in planar solid oxide fuel cells. *J Power Sources* 2009;**190**:402–7.
39. Yang Z, Stevenson JW, Meinhardt KD. Chemical interactions of barium–calcium–aluminosilicate-based sealing glasses with oxidation resistant alloys. *Solid State Ionics* 2003;**160**:213–25.
40. Le S, Sun K, Zhang N, Shao Y, An M, Fu Q, et al. Comparison of infiltrated ceramic fiber paper and mica base compressive seals for planar solid oxide fuel cells. *J Power Sources* 2007;**168**:447–52.
41. Chou YS, Stevenson JW, Gow RN. Novel alkaline earth silicate sealing glass for SOFC. Part II. Sealing and interface microstructure. *J Power Sources* 2007;**170**:395–400.
42. Chou YS, Stevenson JW. Long-term ageing and materials degradation of hybrid mica compressive seals for solid oxide fuel cells. *J Power Sources* 2009;**191**:384–9.